Journal of Cellular Physiology

Acetylation-Dependent Nuclear Arrangement and Recruitment of BMI1 Protein to UV-Damaged Chromatin

GABRIELA ŠUSTÁČKOVÁ,[1] STANISLAV KOZUBEK,[1] LENKA STIXOVÁ,[1] SOŇA LEGARTOVÁ,[1] PAVEL MATULA,[1,2] DARYA ORLOVA,[1] AND EVA BÁRTOVÁ[1]*

[1]*Institute of Biophysics, Academy of Sciences of the Czech Republic, Brno, Czech Republic*

[2]*Faculty of Informatics, Masaryk University, Brno, Czech Republic*

Polycomb group (PcG) proteins, organized into Polycomb bodies, are important regulatory components of epigenetic processes involved in the heritable transcriptional repression of target genes. Here, we asked whether acetylation can influence the nuclear arrangement and function of the BMI1 protein, a core component of the Polycomb group complex, PRC1. We used time-lapse confocal microscopy, micro-irradiation by UV laser (355 nm) and GFP technology to study the dynamics and function of the BMI1 protein. We observed that BMI1 was recruited to UV-damaged chromatin simultaneously with decreased lysine acetylation, followed by the recruitment of heterochromatin protein HP1β to micro-irradiated regions. Pronounced recruitment of BMI1 was rapid, with half-time $\tau = 15$ sec; thus, BMI1 is likely involved in the initiation step leading to the recognition of UV-damaged sites. Histone hyperacetylation, stimulated by HDAC inhibitor TSA, suppression of transcription by actinomycin D, and ATP-depletion prevented increased accumulation of BMI1 to γH2AX-positive irradiated chromatin. Moreover, BMI1 had slight ability to recognize spontaneously occurring DNA breaks caused by other pathophysiological processes. Taken together, our data indicate that the dynamics of recognition of UV-damaged chromatin, and the nuclear arrangement of BMI1 protein can be influenced by acetylation and occur as an early event prior to the recruitment of HPβ to UV-irradiated chromatin.

J. Cell. Physiol. 227: 1838–1850, 2012.

Polycomb group (PcG) proteins are negative regulators of transcription. They play important roles during development, X-chromosome inactivation, and control of cell proliferation (Jacobs and van Lohuizen, 2002). Trithorax group (TrxG) proteins have been described as transcriptional agonists that maintain the active state of gene expression (Lund and van Lohuizen, 2004). A functional link between PcG, TrxG proteins and gene expression has been intensively studied in *D. melanogaster* and *S. cerevisiae*. Studies in *D. melanogaster* have revealed that PcG is required for transcriptional repression of *HOX* genes during development (Ringrose and Paro, 2004). Recent observations have pointed towards an important role for PcG in the mammalian genome (Laible et al., 1997). In the human genome, PcG-regulated gene expression is important for many aspects of development. Moreover, increased expression of PcG proteins correlates with the malignancy and invasiveness of cancer cells (Jacobs and van Lohuizen, 2002; Sauvageau and Sauvageau, 2008).

PcG proteins are compartmentalized within the interphase nucleus into several distinct foci (Buchenau et al., 1998; Saurin et al., 1998) considered to be repression domains of gene transcription. A close physical proximity of chromosomes, such as occurs with "gene kissing" (Kioussis, 2005; Lanctôt et al., 2007), has been described for endogenous PcG target genes and is thought to contribute to transcriptional repression events. The physical association of these genes may occur at PcG bodies, which dictate their transcriptional activity/inactivity (Bantignies et al., 2003). PcG proteins are organized into two main repression complexes, including Polycomb repressive complex 2 (PRC2), in *Drosophila* consisting of Enhancer of zeste (E(z)), Suppressor zeste 12 Su(z)12, Extra sex combs (Esc) proteins, and nucleosome remodeling factor Nurf55 (or EED, EZH2, SU(Z)12, YY1) (Czermin et al., 2002; Müller et al., 2002; Kuzmichev et al., 2004). The PRC1 complex includes proteins such as HP, PSC, RING1, and BMI1 (Lund and van Lohuizen, 2004; Ringrose and Paro, 2004). Recently, the PRC3 complex was described by Kuzmichev et al. (2004) as a complex also containing histone lysine methyltransferase (HMT) EZH2, the HMT activity of which is directed towards histone H3 at lysine

Abbreviations: CENP-A, centromere protein A; ChIP, chromatin immunoprecipitation; DFC, dense fibrillar compartment; DMEM, Dulbecco's Modified Eagle's Medium; DNMT, DNA methyltransferase; DSBs, double strand breaks; FRAP, fluorescence recovery after photobleaching; GFP, green fluorescence protein; h, hour; HATs, histone acetyltransferases; HDACs, histone deacetylases; HP1, heterochromatin protein 1; K (K4, K9, K27. . .), lysine; PBS, phosphate-buffered saline; PcG, polycomb group proteins; PCR, polymerase chain reaction; rDNA, ribosomal DNA; RT, room temperature; TrxG, Trithorax Group proteins; TSA, Trichostatin A.

Conflict of interest statement: The authors declare that there are no conflicts of interest.

Additional Supporting Information may be found in the online version of this article.

Contract grant sponsor: Ministry of Education Youth and Sports of the Czech Republic;
Contract grant numbers: LC535, LC06027, ME 919.
Contract grant sponsor: Academy of Sciences of the Czech Republic;
Contract grant numbers: AVOZ50040702, AVOZ50040507.
Contract grant sponsor: Marie Currie EU project
Contract grant numbers: PIRSES-GA-2010-269156-LCS

*Correspondence to: Eva Bártová, Institute of Biophysics, Academy of Sciences of the Czech Republic, v.v.i., Královopolská 135, CZ-612 65 Brno, Czech Republic. E-mail: bartova@ibp.cz

Received 7 February 2011; Accepted 16 June 2011

Published online in Wiley Online Library (wileyonlinelibrary.com), 5 July 2011.
DOI: 10.1002/jcp.22912

27 (H3K27) and H1(K26) (Kuzmichev et al., 2004). PRC complexes have specific functions within the genome. Factors contained in PRC2 are preferentially responsible for the specific methylation of H3K27 (Cao and Zhang, 2004; Kuzmichev et al., 2004). For example, in *HOX* gene silencing, EED-EZH2 (component of PRC2) mediates H3K27 trimethylation (H3K27me3), which recruits the PRC1 complex through the binding of the Polycomb chromodomain homolog of PRC1 to H3K27me3. Recruitment of PRC1 enables chromatin condensation and prevents access of other chromatin remodeling complexes to the target DNA, leading to gene silencing (Cao and Zhang, 2004). It has been shown that EED-EZH2 mediates H3K27 methylation, but not H3K9 methylation, which is another mark of transcriptionally silent chromatin (Cao et al., 2002; Czermin et al., 2002; Kuzmichev et al., 2002; Plath et al., 2003; Silva et al., 2003). However, whether factors of PcG bodies contribute to the presence of H3K9 methylation, which provides a binding site for heterochromatin protein 1 (HP1), has yet to be resolved (discussed by Cao and Zhang, 2004). Intriguingly, HP1 protein sub-types (HP1α, HP1β, HP1γ) are preferentially responsible for heterochromatin formation, but these proteins were also found to be recruited to UV-induced DNA double strand breaks (DSBs). This event is mediated via the chromoshadow domain of HP1 (Luijsterburg et al., 2009). DSBs are not only bound by phosphorylated histones H2AX (γH2AX), but the phosphorylation of HP1β on amino acid Thr51 accompanies the mobilization and release of HP1β to chromatin with DSBs. This can be suppressed by an inhibitor of casein kinase 2 (Ayoub et al., 2008). Hypothetical interactions between H3K9 methylation-HP1 and PcG-related proteins led to our presumption that PcG proteins may also recognize UV-damaged chromatin.

PcG-related maintenance of gene silencing is conferred through not only structural functions, such as organization of PcG-related proteins to PcG bodies, but also chromatin compaction and the shifting of silenced loci into heterochromatin compartments. For example, PRC1 proteins accumulate at pericentric heterochromatin (Saurin et al., 1998; Luijsterburg et al., 2009). Moreover, human PcG bodies preferentially associated with specific DNA repeats map to the 1q12 region and human chromosomes 9, 15, and 16 (Saurin et al., 1998; Sewalt et al., 2002). Co-localization of PcG bodies with pericentric heterochromatin has been observed in various human cell types. However, the functional significance of this structural phenomenon is not clear (Damelin et al., 2006). This observation supports the hypothesis that PcG-related proteins interact with HP1 proteins that mainly reside at pericentric heterochromatin (Minc et al., 1999, 2001). Moreover, PcG-mediated transcriptional repression and the association of PcG proteins with heterochromatin is not a passive epigenetic event, but a dynamic process. This idea is also supported by the fact that PcG protein complexes actively participate in gene silencing, and BMI1 forms at least two kinetically distinct fractions (Hernández-Muñoz et al., 2005). In addition, the maintenance of DNA methyltransferase 1 (DNMT1) is necessary for proper PcG body nuclear arrangement and function, which is independent of DNMT-associated histone deacetylase activity (Hernández-Muñoz et al., 2005). Based on the results of these previous experiments, we studied the histone acetylation-related kinetics of BMI1 oncoprotein in U2OS cells stably expressing GFP-BMI1. We also focused on the role of BMI1 in the recognition of UV-damaged chromatin, owing to the presumption that BMI1 could also be involved in DNA repair machinery, similar to HP1 sub-types (Ayoub et al., 2008; Luijsterburg et al., 2009; Baldeyron et al., 2011). Our studies revealed that histone hyperacetylation can influence the nuclear arrangement of PcG bodies and disrupt the recognition of UV-damaged chromatin by BMI1 oncoprotein and heterochromatin protein HP1β.

Materials and Methods

Cell cultivation

Human U2OS cells stably expressing GFP-BMI1 originate from the laboratory of Prof. Maarten Van Lohuizen, The Netherlands Cancer Institute, Antoni van Leeuwenhoek Ziekenhuis, Amsterdam, The Netherlands. Cells were provided by Assoc. Prof. Dušan Cmarko, Charles University in Prague. Interphase patterns of exogenous and endogenous BMI were verified by confocal microscopy, which confirmed co-localization of GFP-BMI1 with H3K27me3 (Supplement 1A). For detection of BMI protein, we used anti-BMI, clone F6 (#05-637, Millipore, Consett, UK; see Supplement 1B) and co-localization of GFP-BMI1 with other PcG-related proteins was verified by additional immunofluorescence; we used anti-PHC1 (P13; sc-138523) and anti-Mel18 (H-115; sc-10744; Supplement 1C).

The cells were cultivated in D-MEM with 10% fetal calf serum to 70% confluence, and then treated with a final concentration of 100 nM Trichostatin A (TSA) or 15 μM SAHA. Both agents caused histone hyperacetylation (Supplement 2A; TSA-induced hyperacetylation was conserved even when cells went through mitosis. SAHA significantly increased H3K9 acetylation, similar to TSA, not shown).

The same cultivation conditions used for GFP-BMI-U2OS cells were applied to mouse 3T3 cells stably expressing HP1β (a generous gift from Dr. Paul Verbruggen from Swammerdam Institute for Life Sciences, University of Amsterdam, The Netherlands). Cells were cultured at 37°C in a humidified atmosphere containing 5% CO_2. For the FRAP technique, the cells were seeded on uncoated, gamma-irradiated, 50-mm Glass Bottom Dishes (No. 0), used for inverted microscopy (MatTek Corporation, Ashland, MA, #P50G-0-30-F). Hoechst 33342 (0.4 μg/ml) was used for counterstaining and vital visualization of interphase nuclei. Hoechst 33342 was only used to verify the shape and condition of nuclei in living cells, not in DNA damage experiments where Hoechst 33342 can be used for cell sensitization before micro-irradiation with a 405 nm laser (we did not use this approach).

Induction of DNA double stand breaks

U2OS cells stably expressing GFP-BMI1 and 3T3 cells stably expressing EGFP-HP1β were cultivated under standard conditions. At 70% confluence, the cells were sensitized with 10 μM 5-bromo-2′-deoxy-uridine (BrdU), 1–18 h before local irradiation. Control and TSA-treated U2OS and 3T3 cells were stained using the BrdU Labeling and Detection Kit I (#11296736001, Roche, Prague, CZ). Control detection of BrdU incorporation was performed, according to the manufacturer's protocol. We observed an identical level and nuclear pattern of BrdU incorporation in control and TSA-treated U2OS cells (Supplement 2B). BrdU-sensitized cells were irradiated by UV laser (355 nm). We irradiated half of the nuclei or defined strips (Fig. 1A) by 80% laser output, not reduced at acousto-optic tunable filter (AOTF). The following settings were used: 512 × 512 pixels, 400 Hz, bidirectional mode, 64 lines, zoom >5–10. Irradiated cells were fixed in 4% paraformaldehyde and phosphorylated histone H2A.X (γH2AX) was detected with rabbit polyclonal antibody against γH2A.X (phospho S139; #ab2893, Abcam, Cambridge, UK) in immunofluorescence and confocal microscopy (Fig. 1A).

Fluorescence recovery after photobleaching (FRAP) and image analysis

These experiments were performed using confocal microscope Leica TSC SP-5X, equipped with white light laser (WLL, 470–670 nm in 1-nm increments); argon laser (488 nm), and UV lasers

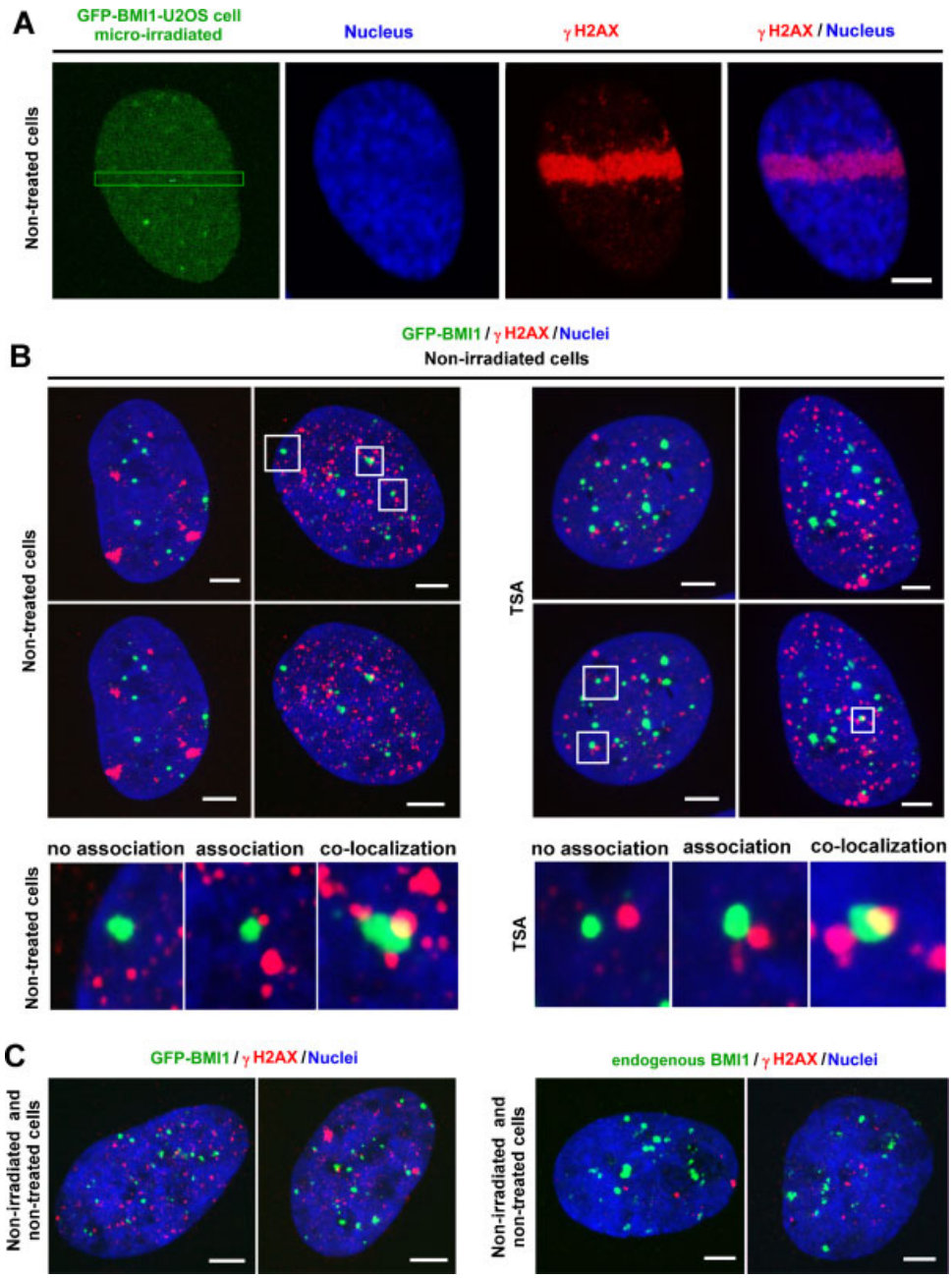

Fig. 1. Recruitment of BMI1 protein to UV-damaged chromatin induced by micro-irradiation. A: GFP-BMI1-U2OS (green) cells were micro-irradiated by UV laser (355 nm) and the induction of DSBs was verified using antibody against γH2AX (red strip). Bar represents 4 μm. B: The presence of γH2AX was detected in both non-irradiated control and TSA-treated cells. Bars represent 4 μm. No co-localization, association, or strict co-localization was found for GFP-BMI1 protein (green) and γH2AX (red). See selected frames. C: Degree of co-localization between BMI1 (green) and γH2AX (red) was studied for both exogenous (GFP-BMI1) and endogenous BMI1. Bars represent 4 μm.

(405 and 355 nm). We used a magnification of 64×/NA = 1.4. The cells were placed in a cultivation hood (EMBL Heidelberg, Germany), heated to 37°C. In addition, we used a specific "Air Stream" incubator to get 5% CO_2 for optimal cell cultivation.

Excitation for image acquisition of BMI1-GFP was set to 496 nm at WLL; photobleaching was set to 488 nm using the argon laser. One detector was used for the detection of GFP green light (in the region above 496 nm); the second detector was set for transition light, which enabled better finding of the focal plane. Leica-designed software was used for data acquisition in live data mode (LDM), in which two scanning modes were defined; the first mode for bleaching using argon laser and the second mode for stack acquisition using WLL. The resolution was 512 × 512 pixels/400 Hz; bidirectional scanning was used, and line averaging was set to 8 to increase the time interval for bleaching to 1 sec; the power of argon laser was set to 70%. The power of WLL was used as low as possible (5%) in order to limit the image intensity during the time interval (600 sec). The zoom for bleaching was high (>10) in order to get sufficient power to the bleached area. The second scanning mode was used for stack acquisition, setting the lower and upper limits to ±1.5 μm relative to the focal plane. The number of lines was 2; the number of sections was 10; the time interval between

stacks was minimized (~13 sec); the number of stacks was 50. The transition of image parameters from one scanning mode to the other was enabled by setting Galvano position and x–y stage for LDM.

Analysis of the acquired images was performed using LEICA LAS AF, version 2.1.2. software. The 3D images were used to calculate the maximum image for each stack. Owing to the slight motion of living cells, the maximum image from time series was also subsequently calculated. The resulting image enabled a precise setting of regions of interest (ROIs) that involved bleached foci for any time interval. The time series of average intensities were calculated inside ROIs. The background was determined using ROI as near to the bleached point as possible but inside the cell nucleus for the whole time interval. The background intensity was subtracted from signal and normalized to the initial value of the intensity before bleaching. The kinetics of the fluorescence recovery was fitted by means of simple exponential equation with three parameters (F-final value of the fluorescence, A-amplitude of recovery, which was very near to F, and τ—time of recovery). The final value was always lower than the initial intensity before bleaching. Experiments were repeated six times and the time series for control and TSA treated cells were analyzed by SigmaPlot software. Average values from FRAP experiments are shown with standard deviations.

Segmentation of nuclei

Fixed cells nuclei (blue channel) were segmented using an algorithm based on edge detection. First, the images were smoothed using a Gaussian filter with anisotropic variance (we used $\sigma x = \sigma y = 1.5$, $\sigma z = 1$). Fast infinite impulse response (IIR) implementation of the Gaussian filtering was used. Then, the magnitude of image gradient was computed using a central difference approximation formula. The edges were identified as the voxels having the gradient magnitude bigger than 1% of the maximal gradient magnitude in the image. The connected components of the edge voxels formed objects' shells (often with many holes). The shells having large enough bounding boxes (i.e., the bounding box volume was bigger than 100,000 voxels) were considered nuclear shells. Every big shell was morphologically closed with a spherical structuring element of 3-μm radius. The holes that should have remained in the closed shells were filled on every slice. The Gaussian smoothing slightly dislocated the edges; therefore, we eroded the binary mask by 0.3 μm.

PcG body segmentation

Polycomb bodies were searched for in the green channel within the space identified by nuclear segmentation. First, we applied morphological top-hat transformation with a spherical structuring element of size 2 μm. Then we set the image threshold with automatically determined threshold (we used 80% of the peak intensity in top-hat image). The peak intensity was given by 99.5 intensity percentile. We discriminated the objects by size, only taking those that had volumes bigger than 80 voxels^3.

We studied the number of polycomb sites in every nucleus, the volume of the polycomb sites, and local nuclear radii (defined by Uhlířová et al., 2010). Owing to the fact that, in control cells, we observed polycomb sites of two significantly different sizes, we studied the local radius measured for small, as well as large, polycomb sites. We used a value of 22 for size classification. This value was chosen because it lies between two imaginary peaks in Figure 7C. Any other value between 20 and 28 would work as well, because there were no PcG bodies with volumes in that interval.

Cell cycle measurements

The cells were fixed in 70% ethanol and stored at -20°C. Prior to measurement, the cells were washed twice in PBS and stained with propidium iodide (10 μg/ml), dissolved in Vindelov's solution (1 mM Tris–HCl [pH 8.0], 1 mM NaCl, 0.1% TritonX-100, 10 μg/ml RNase A). Cells were then incubated for 30 min at 37°C. For analysis, we used the FASCalibur flow cytometer (Becton Dickinson, Franklin Lakes, NJ), controlled by CellQuest software running on an Apple Macintosh computer. ModFit software (Verity Software House, Topsham, ME) was used for cell cycle analysis.

Immuno-fluorescence

Cells were fixed in 4% paraformaldehyde (PFA) for 10 min at room temperature (RT), permeabilized with 0.2% Triton X-100 for 10 min, and with 0.1% saponin (Sigma–Adrich, Prague, Czech Republic) for 12 min, and washed twice in PBS for 15 min. We used 1% BSA dissolved in PBS as a blocking solution. After 1 h of incubation in BSA, the slides were washed for 15 min in PBS, and incubated with the following antibodies: anti-HP1α (clone 15.19s, #05-689, Upstate, Temecula, CA), anti-HP1β (#07-333, Upstate and #MAB3448, Chemicon International, Hofheim, Germany), anti-HP1γ (clone 42s2, #05-690, Upstate), anti-H3K27me3 (#07-449, Upstate), and Acetyl Lysine Antibody-ChIP Grade (#21623, Abcam). Immunocytochemistry was performed according to Harničarová et al. (2006), Harničarová Horáková et al. (2010), and Bártová et al. (2008).

Confocal microscopy and analysis of nuclear radial distribution for PcG bodies

Image acquisition of fixed preparations was done using a Nipkow-disc based confocal microscope. The acquisition procedure is decribed in Bártová et al. (2008). The image acquisition system was controlled by FISH 2.0 software (Kozubek et al., 1999) and 3D-image visualization was done using Aquiarium software (http://cbia.fi.muni.cz/acquiarium.html).

Western blotting

After washing the cells with PBS, they were lysed in sodium dodecyl sulphate (SDS)-lysis buffer (50 mM Tris–HCl, pH 7.5; 1% SDS; 10% glycerol) and the next steps were performed as in Bártová et al. (2005) and Harničarová et al. (2006). For Western blotting, we used the same primary antibodies as for immunofluorescence. For detection of the BMI1 levels, we used monoclonal antibody against BMI1, clone F6 (#05-637, Millipore). For analysis of PcG-related proteins we used following antibodies: PHC1 (P13; sc-138523); RING1 (H-110; sc-28736); M33 (C-18; sc-19297); Mel18 (H-115; sc-10744). As a secondary antibody, we used anti-rabbit IgG (A-4914, Sigma, Munich, Germany; dilution 1:2,000), anti-mouse IgG (A-9044, Sigma; dilution 1:2,000), or anti-mouse IgG_1 (sc-2060, Santa Cruz Biotechnology, Inc., Heidelberg, Germany; dilution 1:500). After immuno-detection, each membrane was stained with amidoblack to confirm equal protein loading.

Immunoprecipitation experiments

The protocol for immunoprecipitation was modified according to Dawson et al. (2009). Cytoplasmic, and nucleosolic fractions were prepared. We used the following buffers: (A) 10 mM HEPES (pH 7.9), 1.5 mM $MgCl_2$, 10 mM KCl, 0.5 mM DTT and protease inhibitor cocktail (aprotinin 1 mg/ml, PMSF 500 mM). (B) 20 mM HEPES (pH 7.9), 1.5 mM $MgCl_2$, 300 mM NaCl, 0.5 mM DTT, 25% (v/v) glycerol, 0.25% Triton X-100, 0.2 mM EDTA, prothease inhibitor cocktail. (C) IPH buffer: 150 mM NaCl, 50 mM Tris–HCl (pH 8.0), 5 mM EDTA, 0.5% (v/v) Nonidet P40. Fraction containing chromatin and chromatin-associated proteins was lysed by IPH buffer, sonicated and were incubated with the appropriate antibodies (anti-HP1β, #07-333, Upstate; Acetyl Lysine Antibody-ChIP Grade, #21623, Abcam). Incubation proceeded overnight, then agarose A-beads were added, and the incubation was continued for another 4 h at 4°C, followed by washing with IPH buffer for 5 min. Then, 25–50 μl of 2$\times$ Laemmli buffer was added to the sediment. The samples were boiled 5 min at 95–100°C and then centrifuged at 700 rpm. The extracted proteins were separated by SDS–PAGE, and transferred to polyvinylidene difluoride (PVDF)

membranes (BioRad). For detection of BMI1 protein, we used a monoclonal antibody against BMI1, clone F6 (#05-637, Millipore). HP1β protein and lysine acetylation were detected with antibodies described above.

HDAC1 siRNA

To verify the effect of HDAC inhibition on the recruitment of proteins to UV-damaged chromatin, we purchased human HDAC1 siRNA from Santa Cruz Biotechnology, Inc. (#sc-29343). Cell transfection was done by 4D Nucleofector (Lonza Cologne, GmbH, Cologne, Germany), according to the manufacturer's instructions. We used the SF Cell Line Nucleofector X Kit (V4XC-2032) and optimal amounts of HDAC1 siRNA (300 nM). After transfection with 4D Nucleofector, the cells were incubated for 24 h at 37°C in a CO_2 incubator in standard cultivation medium. Transfection efficiency was confirmed by Western blots and immunofluorescence. To verify HDAC1 levels, we used the recommended antibody HDAC1 (H-51; #sc-7872). We used dilution 1:500 for Western blots and 1:50 for immunofluorescence.

ATP depletion

We used a protocol adopted from to Kruhlak et al. (2006). ATP depletion was verified by Mitotracker (Invitrogen, Carlsbad, CA) staining that showed changes in mitochondrial morphology.

Results

BMI1 protein is recruited to UV-damaged chromatin induced by local irradiation

Double strand breaks (DSBs) were induced by 355-nm UV laser and, following local DNA damage, the presence of phosphorylated H2.AX (γH2A.X) was detected as a marker of chromatin with DSBs (Fig. 1A). When we analyzed γH2A.X in non-irradiated cells by high resolution Nipkow-disc confocal microscopy, we also observed γH2A.X positive regions (red signals in Fig. 1B). In non-irradiated cells, we analyzed the relationship between γH2A.X (red) and PcG bodies (green; Fig. 1B). We observed all possibilities: BMI1 and γH2A.X foci that did not co-localize, and foci that were associated or co-localized (magnification in lower parts of Fig. 1B). These data confirm that γH2A.X positivity is not solely a response to ionizing radiation. The appearance of γH2A.X in non-irradiated cells could be a consequence of other cellular processes, including apoptosis, replication fork collision, or the dysfunctional telomeres that can appear in tumor cells, including the osteosarcoma U2OS cell line (summarized by Fernandez-Capetillo et al., 2004; Fillingham et al., 2006). After TSA addition, no significant differences in γH2A.X nuclear distribution in non-irradiated cells were observed compared to the relevant control. This corresponds to insignificant apoptosis that may occur at marginal levels in both control and TSA-treated cells. In U2OS cells, Ismail et al. (2010) mentioned the existence of domains that are positive for both γH2A.X and BMI1 in non-irradiated cells. We confirmed this possibility (see magnification in Fig. 1B, yellow signals), but the number of foci with co-localized γH2A.X and BMI1 was low; only ~10%. Thus, we suggest that BMI1 has slight ability to recognize γH2A.X positive DNA lesion that arise spontaneously, for example due to replication stress. This conclusion was confirmed when we compared the nuclear pattern of GFP-tagged BMI and γH2A.X positive regions with the nuclear distribution of endogenous BMI1 and γH2A.X positive chromatin (Fig. 1C).

After confirming the status of γH2A.X in control and TSA treated non-irradiated cells, we aimed to determine whether the BMI1 protein recognizes irradiation-induced DNA damage. We observed an increased accumulation of BMI1 to sites of DNA damage following micro-irradiation in several cells (Fig. 2Aa). The increased accumulation of BMI1 at DSBs occurred rapidly ($\tau = 15$ sec) compared to another heterochromatin-related protein HP1β, which was detected at DSBs from 100 to 800 sec (Ayoub et al., 2008; Luijsterburg et al., 2009). The appearance of high levels of BMI1 at chromatin with DSBs was accompanied by stable levels of H3K27me3, which is a PRC1 binding partner (Fig. 2B). Pronounced recruitment of BMI1 to UV-damaged chromatin was observed in living cells that were stably or transiently expressing BMI1. In addition, this was confirmed for both exogenous and endogenous BMI1 (not showed). However, our experiences are in agreement with Hong et al. (2008) explaining that the weak appearance of endogenous PcG-related proteins at UV-damaged chromatin is probably due to methodological limits of immuno-fluorescence, including the low sensitivity of antibodies and/or rapid dissociation of PcG-related proteins from sites of their pronounced accumulation.

Acetylation-dependent recruitment of BMI1 to UV-damaged chromatin

When the cells were treated with HDAC inhibitor, TSA, no increased accumulation (nor a complete absence) of BMI1 at DSBs was detected (Fig. 2Ab). A similar effect of histone hyperacetylation (Fig. 2C) on BMI1 recruitment to UV-damaged chromatin was confirmed after SAHA cell treatment and by degradation of HDAC1 mRNA by siRNA. Similarly to cells with reduced levels of HDAC1 by siRNA, cells treated with HDAC inhibitor SAHA showed an absence of BMI1 accumulation at UV-damaged chromatin (Fig. 2Ac or compare Fig. 2Ad1 with control Fig. 2Ad2). These data confirmed the importance of histone acetylation in DNA repair process. However, the level of BMI1 acetylation must be also taken into account. We observed by immunoprecipitation that TSA treatment reduced BMI acetylation (Fig. 3C), which is the opposite effect as occurred for histone hyperacetylation in response to TSA (Supplement 2A). Intriguingly, the acetylation of all lysines was low when BMI1 had markedly accumulated at UV-damaged chromatin (Fig. 2D). Collectively, these experiments point to acetylation events as important players in the recognition of UV-damaged chromatin.

HP1β accumulates at UV-damaged chromatin more slowly than BMI1, but HDACi prevents the increased accumulation of both BMI1 and HP1β at this genomic region

Following the results of the immunofluorescence and imunoprecipitation experiments, showing that BMI1 is a potential binding partner for HP1β (Fig. 3A,B). We asked whether BMI1 and HP1β interact at UV-damaged chromatin. HP1β accumulated at damaged regions slowly (200 sec after irradiation; Fig. 4A, Luijsterburg et al., 2009) compared to BMI1, which began to accumulate at UV-damaged genomic regions within 15 sec (Fig. 2Aa). Similar to BMI1, increased accumulation of HP1β was observed in cells transiently (not shown) or stably expressing GFP-HP1β (Fig. 4A).

Inhibition of histone deacetylases by TSA prevented the recruitment of both BMI1 and HP1β proteins to damaged chromatin (Figs. 2A and 4A), which implies that the role of both BMI1 and HP1β at UV-damaged chromatin could be similarly influenced by changes in global protein acetylation induced by TSA (Supplement 2A and Fig. 2D; Tóth et al., 2004; Bártová et al., 2005). Based on this observation, it seems to be evident that not only histone acetylation, but also acetylation of non-histone proteins could play a role in DNA repair.When we performed immunoprecipitations with antibody against all acetylated lysines, we observed a reduced level of acetylation for BMI1 after TSA treatment (Fig. 3C). This was different from the histone hyperacetylation caused by TSA (Supplement 2A).

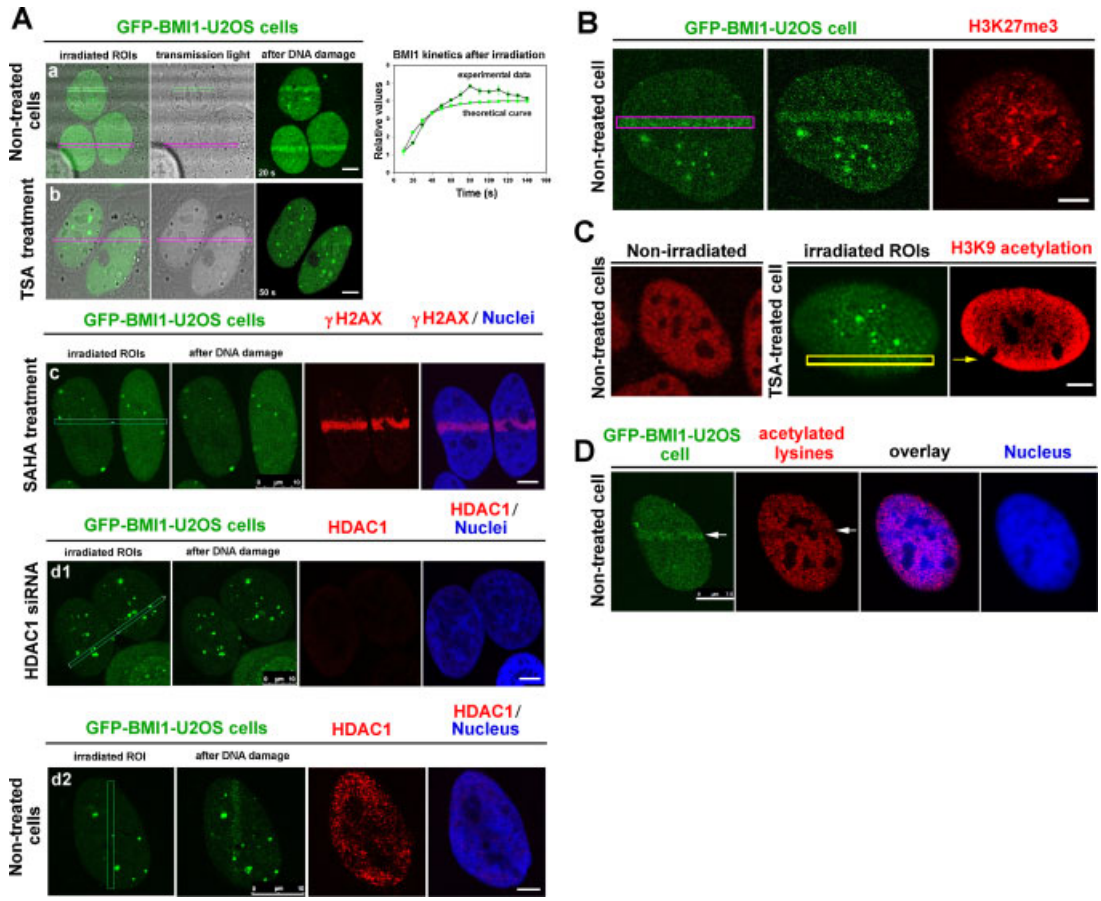

Fig. 2. Acetylation-dependent recruitment of BMI1 protein to UV-damaged chromatin. Aa: Live control GFP-BMI1-U2OS cells were monitored for 100 sec after irradiation and BMI1 accumulation at DSBs was detected within ~15 sec. Kinetic properties of BMI1 in irradiated control U2OS cells are shown in the enclosed graph. Ab: TSA prevented increased BMI1 accumulation at UV-damaged chromatin. Ac: No recruitment of BMI1 to UV-damaged chromatin after SAHA treatment and (Ad1) after HDAC1 siRNA. Ad2: Part represents non-treated control cells, irradiated by UV laser, with accumulated GFP-BMI (green), and standard level of HDAC1 (red). B: No increased accumulation (but not an absence) of H3K27me3 in micro-irradiated (BMI1-dense) regions in control GFP-BMI1-U2OS cells is shown. C: Association of H3K9 acetylation within micro-irradiated regions, with no increased accumulation of BMI1 (green) at damaged sites in the cells treated by TSA. Level of H3K9 acetylation (red) was low in non-treated cells (left part) in comparison with TSA treated cells (right part). Bars in parts A–C represent 5 μm. D: Antibody against acetylated lysines showed decreased level of all acetylated lysines (red) at UV-damaged chromatin with increased accumulation of BMI1 (green). Bar represents 7.5 μm.

Despite this contradiction, these data do not argue against an important role for acetylation during the repair of UV-damaged chromatin. However, it is hard to distinguish whether histone hyperacetylation or BMI1 hypoacetylation, which appeared simultaneously after TSA treatment, dictate pronounced recruitment of BMI1 to UV-damaged regions.

Other interesting result is that when we inhibited RNA Pol II by actinomycin D, we observed no increased accumulation of BMI1 into UV-damaged chromatin (not shown; it is similar like after TSA addition). This result confirmed the suggestion of Chou et al. (2010) that RNA Pol II-related transcription machinery also participates in DNA repair processes. After TSA or actinomycin D treatment, there was neither increased accumulation nor absence of BMI1 and HP1β at irradiated chromatin. Thus, it was possible to use FRAP to study protein kinetics in irradiated regions (Figs. 4B and 5A).

Kinetics of BMI1 and HPβ at UV-damaged chromatin

We performed photobleaching in laser irradiated areas of control and TSA-treated cells expressing GFP-BMI1 and GFP-HP1β and observed similar recovery properties: TSA did not affect the fluorescence recovery after GFP-BMI1 and GFP-HP1β photobleaching (Figs. 4B and 5A). In addition, for HP1β, we observed similar kinetic properties at UV-irradiated regions when we made distinctions between euchromatin and heterochomatin in control and TSA treated cells (see Fig. 4Ba–d).

Kinetics of BMI1 in PcG bodies is affected by histone hyperacetylation by HDAC inhibitor

FRAP was used to measure the time required for fluorescence recovery after photobleaching. We used time-lapse confocal microscopy and the FRAP module to bleach individual BMI1 foci organized into PcG bodies and away from PcG bodies (Fig. 5B). Image acquisition was performed with the aid of a white laser under transmission light (Fig. 5B). The recovery fluorescence was normalized to 1.0 (further shown as relative fluorescence) and was plotted against time (Fig. 5C). We bleached approximately 20 PcG foci (Fig. 5B, frame and magnification) in six independent experiments and the average values with standard deviations (SD) were plotted (Fig. 5C). In control GFP-BMI1 positive cells, $\tau 5_0$ was observed between 75 and 90 sec,

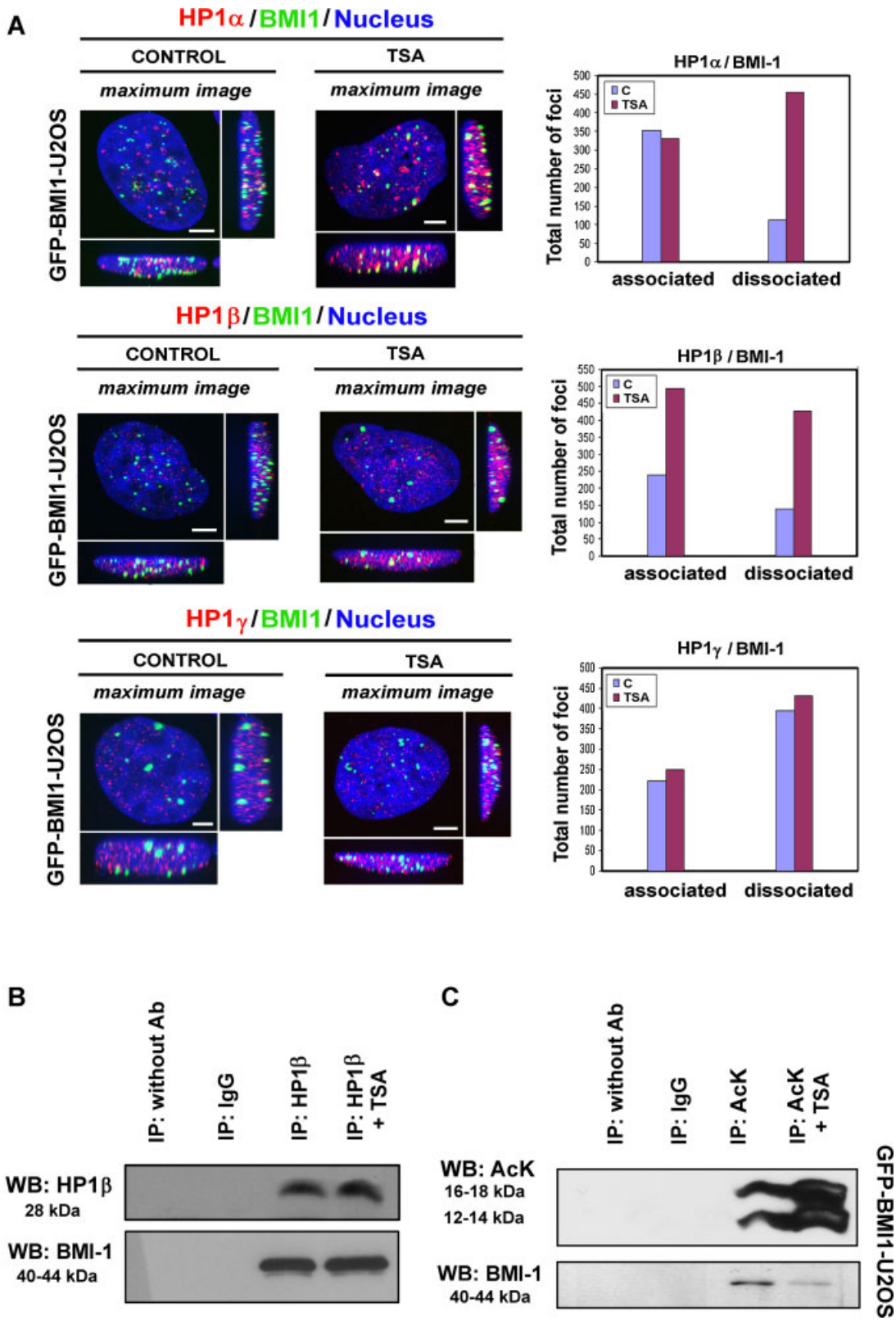

Fig. 3. Relationship of BMI1 to HP1 protein sub-types. A: Relationship of BMI1 (green) and HP1α, HP1β, HP1γ (red) studied by immunofluorescence and the degree of BMI1-HP1 co-localization in control and TSA-treated cells is shown quantitatively in bar graphs. Bars in images represent 5 μm. B: Immunoprecipitation experiments revealed the binding of HP1β to BMI1. TSA had no effect on the interaction between HP1β and BMI1, which can be caused by an increased number of PcG bodies after TSA addition (Fig. 7D) or by changes in BMI1-HP1β co-localization caused by TSA as shown in part A. C: Level of BMI1 acetylation was studied using antibodies against acetylated lysines. As a negative control, we used samples with no antibody and non-specific IgG (Rabbit Control IgG-ChIP Grade, #ab46540, Abcam).

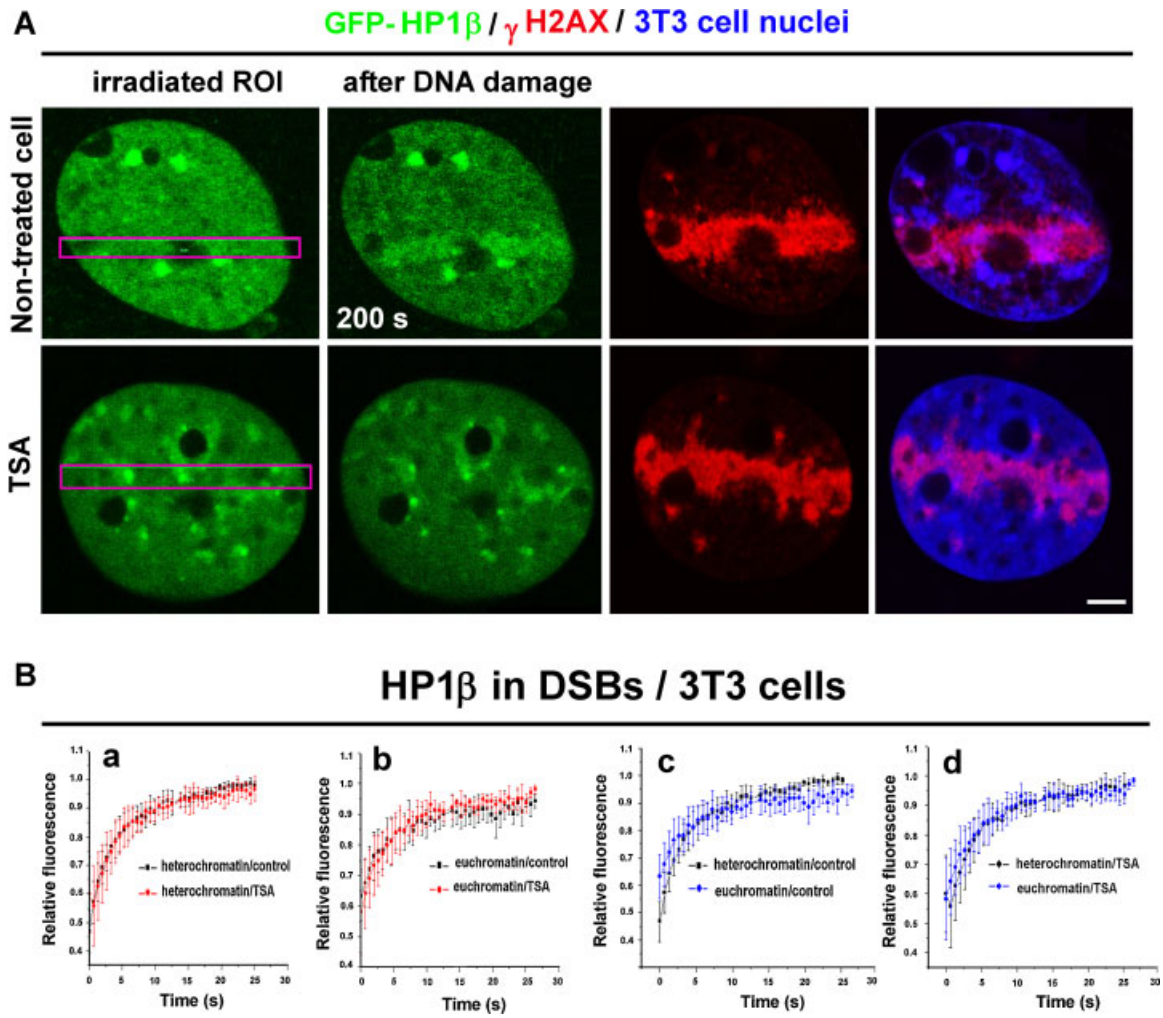

Fig. 4. Recruitment of HP1β to UV damaged chromatin is influenced by the histone acetylation state. A: Live control GFP-HP1β-3T3 cells were micro-irradiated and increased accumulation of HP1β at damaged chromatin was detected within ~200 sec. TSA prevented HP1β recruitment to damaged chromatin, but HP1β was not absent at micro-irradiated regions of TSA treated cells. Bar represents 4 μm. B: FRAP was performed in UV-damaged chromatin (micro-irradiated euchromatin and heterochromatin) of control and TSA-treated GFP-HP1β-3T3 cells. Panel a: A comparison HP1β recovery at heterochromatin of control and TSA treated cells. b: HP1β recovery at euchromatin of control and TSA treated cells. c: A comparison of HP1β recovery at heterochromatin and euchromatin of control cells. d: A comparison HP1β recovery at heterochromatin and euchromatin of TSA treated cells.

while treatment with HDAC inhibitor TSA prolonged the recovery time to 179–250 sec for $\tau 5_0$ (Fig. 5C). These experiments showed that there are multiple dynamic fractions of BMI1 protein and that TSA treatment changes the ration of the freely mobile (outside the PcG bodies) and less mobile fractions in PcG bodies. Moreover, we observed high variability in BMI1 recovery time among individual PcG foci (see standard deviation, SD, in Fig. 5C). When we measured the level of BMI1 outside of PcG bodies, this protein was immediately recovered to the original value (Fig. 5D). These data support the conclusions of Hernández-Muñoz et al. (2005) that described two kinetically different pools of BMI1 protein.

We next asked whether BMI1 kinetics change throughout the cell cycle. Flow cytometric analysis showed that, 4 h after TSA treatment, U2OS cells were blocked in the G1 phase of the cell cycle (Fig. 5E). Due to the feasibility of these experiments, we measured the BMI1 kinetics 24 h after TSA treatment, when decreased level of BMI1 (GFP-BMI1) occurred (Fig. 5F). At this point, cells were blocked in the G2-M phase of the cell cycle (Fig. 5E). Hernández-Muñoz et al. (2005) have published that distinct kinetic states exist for BMI1 in G1 and G2 cells. They showed that, in G1 cells, the recovery time ($\tau 5_0$) is 41 ± 13 sec, while in G2 cells it is 63 ± 17 sec (Hernández-Muñoz et al., 2005). Taking into account the possible influence of cell cycle on protein kinetics, we synchronized GFP-BMI1 U2OS cells by serum deprivation to reproduce the distinct BMI1 kinetics in G1 cells and G2 cells, as published by Hernández-Muñoz et al. (2005). After serum deprivation, the cells lost the GFP fluorescence; thus, we were unable to perform the FRAP experiments. According to Hernández-Muñoz et al. (2005), the recovery time in G1 cells is slower then in G2 cells; thus, a block in G2 (observed in our experimental system 24 h after TSA treatment) could be associated with a rapid recovery time. However, 24 h after TSA treatment, we observed a slower recovery time for BMI1 compared to control cells (Fig. 5C). We can surmise that our data are subtly influenced by the fact that we have analyzed more G2 cells in the TSA-treated cells than in control cells.

The different kinetics of BMI1 after 24 h TSA treatment correlated with changes in the BMI1 status, as determined by

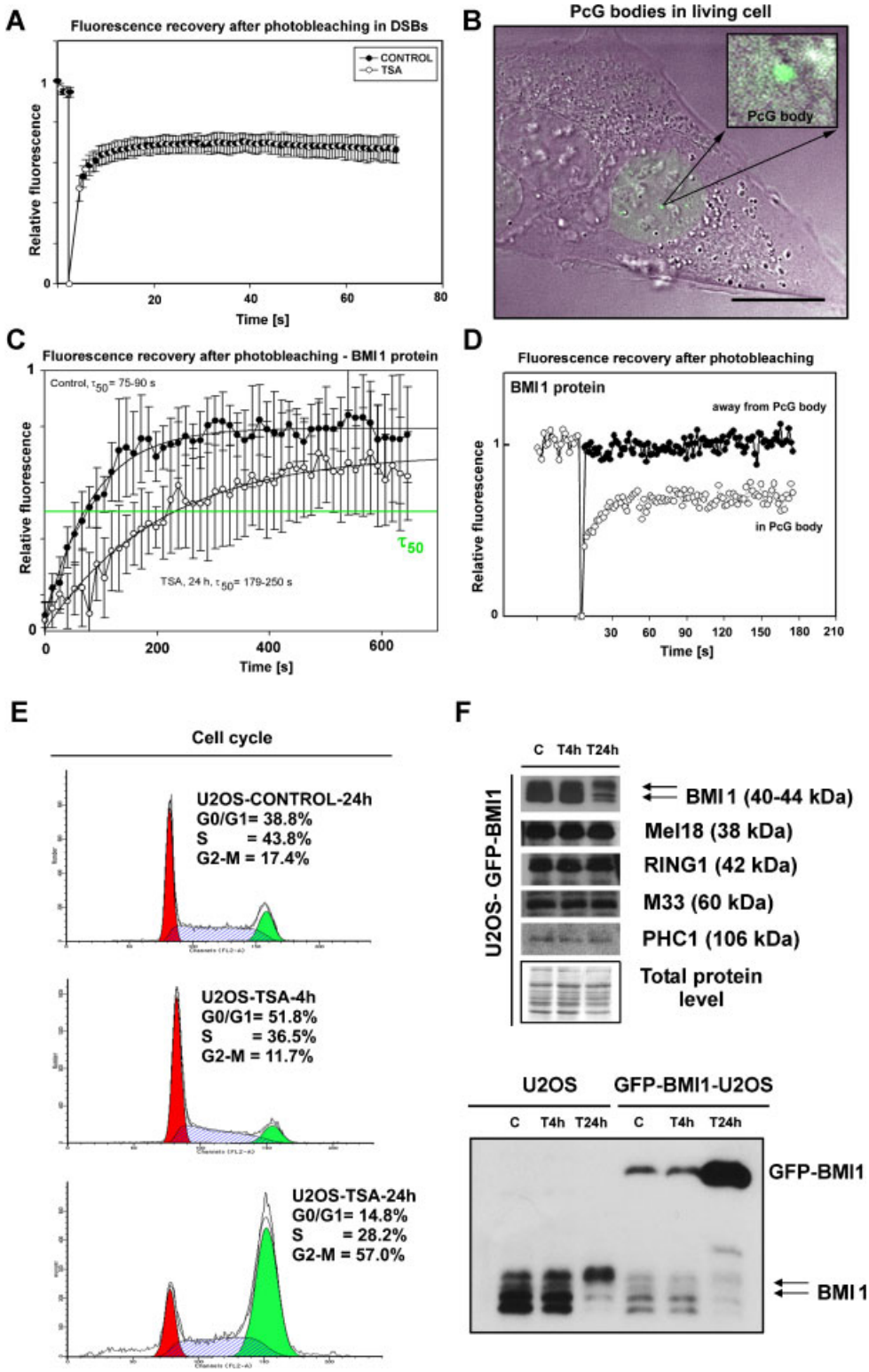

Fig. 5. Kinetics of GFP-BMI1 protein and its relationship to cell cycle changes induced by TSA. A: FRAP was performed in micro-irradiated regions in control and TSA-treated GFP-BMI1-U2OS cells. B: Live U2OS cells stably expressing GFP-BMI1. Frame indicates selected PcG body containing BMI1 protein. Bar represents 18 μm. C: Results of FRAP on GFP-BMI1 protein in control and TSA-treated non-irradiated U2OS cells. Data are shown as relative recovery of fluorescence, normalized to 1.0. (D) Recovery time profile of GFP-BMI1 (accumulated in PcG bodies; unfilled dots) was compared to GFP-BMI1 localized outside of PcG foci (black dots). E: Cell cycle changes induced by TSA in GFP-BMI1-U2OS cells. G1 phase is red, S is blue dashed, and green peaks represent G2/M phase of the cell cycle. F: Western blots detected the levels of PcG-related proteins, BMI1, Mel18, RING1, M33, and PHC1, in untreated cells and cells treated with TSA for 4 and 24 h.

Western blots (Fig. 5F). After 24 h TSA treatment, a reduced level of endogenous BMI1 was observed, however, increased level of GFP-BMI1 was recognized (Fig. 5F, lower part). When we analyzed other PcG-related proteins, including Mel18, RING1, M33, and PHC, by Western blot, we observed no significant changes in their levels after TSA addition compared to non-treated controls (Fig. 5F). Thus, the changes in the levels of BMI1 or GFP-BMI1 after TSA treatment seem to be unique among PRC1-related proteins (Fig. 5F).

ATP depletion and accumulation of BMI1 and HP1β to UV-damaged chromatin

Many published papers have shown the regulatory role of metabolic energy in the movement of chromatin-related proteins (Muratani et al., 2002; Kruhlak et al., 2006). Thus, we examined the recruitment of BMI1 and HP1β to UV-damaged chromatin after induced ATP-depletion. For BMI1, we made some interesting observations: when we irradiated regions with PcG foci, they dispersed (Fig. 6Aa–b). Irradiated regions that were BMI-positive but lacked PcG foci, lack a pronounced accumulation of BMI (Fig. 6Ac). Interestingly, after ATP-depletion, there was a pronounced de-compaction of UV-irradiated chromatin, which we have never observed in irradiated human somatic cells without ATP depletion (compare blue nucleus in Fig. 1A, with Fig. 6A, blue). After ATP depletion, we also measured high levels of γH2AX in whole nuclei (Fig. 6A, staining in red). For HP1β, we observed a similar tendency as for BMI1. There were high levels of γH2AX positivity and no pronounced accumulation of HP1β in UV-damaged chromatin after ATP depletion (Fig. 6B). This observation was completely different from the non-treated control cells (Fig. 4A, upper part).

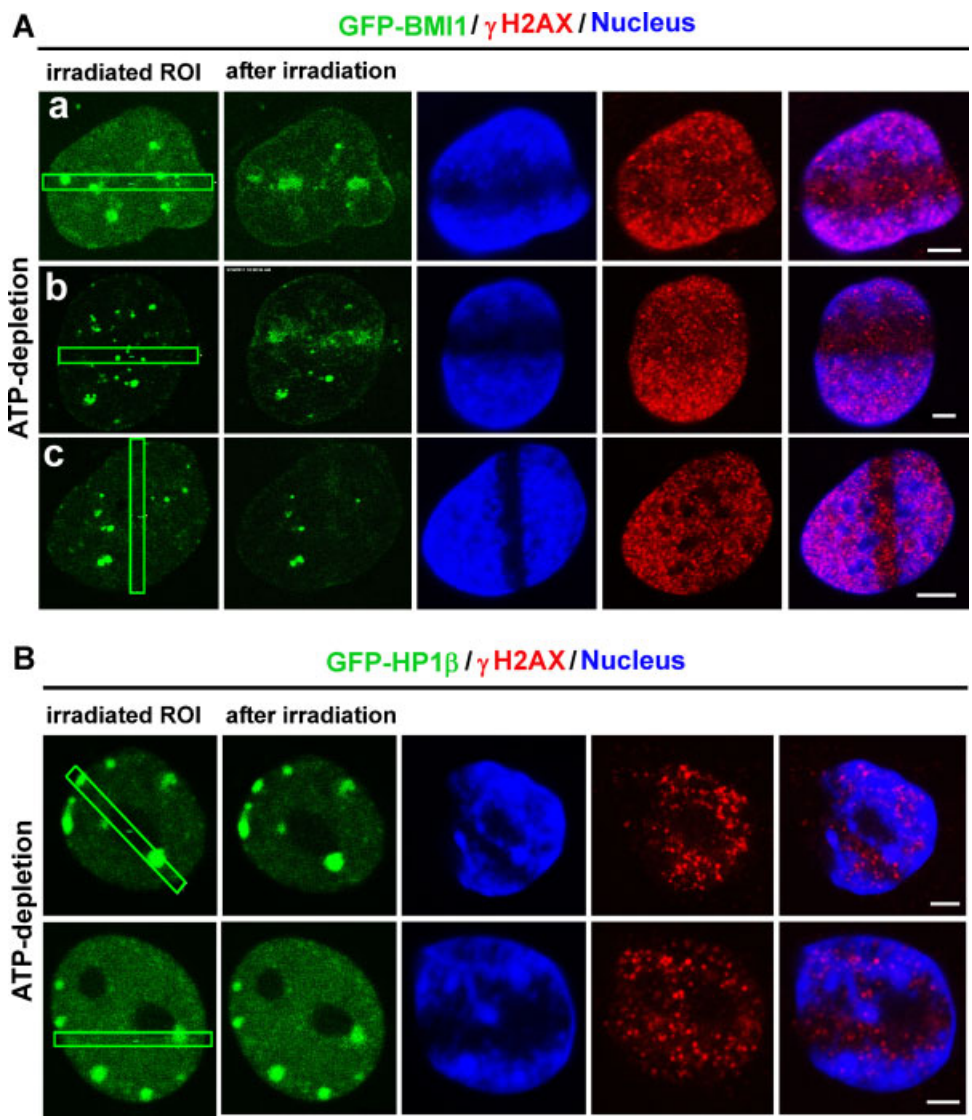

Fig. 6. Recruitment of GFP-BMI1 and HP1β proteins to UV damaged chromatin after ATP depletion. Aa–b: ATP depletion caused the dissociation of BMI1 protein that had accumulated into foci (green). Ac: After ATP depletion, pronounced recruitment of GFP-BMI1 was not observed at irradiated chromatin without PcG bodies. A high degree of chromatin relaxation (blue) occurred after ATP depletion, similar to the high level of γH2AX (red). B: Pronounced recruitment of HP1β to UV-irradiated chromatin was not observed after ATP depletion. Bars represent 4 μm.

Nuclear pattern and nuclear radial distribution of PcG bodies after TSA treatment

We next asked whether histone hyperacetylation influences nuclear arrangement of PcG bodies. Nuclear parameters for GFP-BMI1 protein accumulated in PcG bodies were calculated in control and TSA-treated U2OS cells (Fig. 7A). In control U2OS cells, the average volume of PcG bodies was approximately $19.3 \pm 11.1\ \mu m^3$, while TSA had the ability to reduce PcG volume to $8.2 \pm 2.5\ \mu m^3$ (Fig. 7B). Interestingly, in control cells, we observed two significantly different volumes for PcG bodies (see Fig. 7A and quantification in Fig. 7C), which were completely different from the volume of PcG bodies in TSA-treated cells. When we counted the number of PcG bodies, we observed that this parameter increased from 26.4 ± 2.1 in the control to 33.3 ± 2.0 after TSA treatment (Fig. 7D). The last nuclear parameter that we studied was the nuclear radial positioning of PcG bodies (defined by Uhlířová et al., 2010). We observed that the median of PcG location is approximately 80% of the nuclear radius and that TSA did not change this nuclear parameter (Fig. 7E).

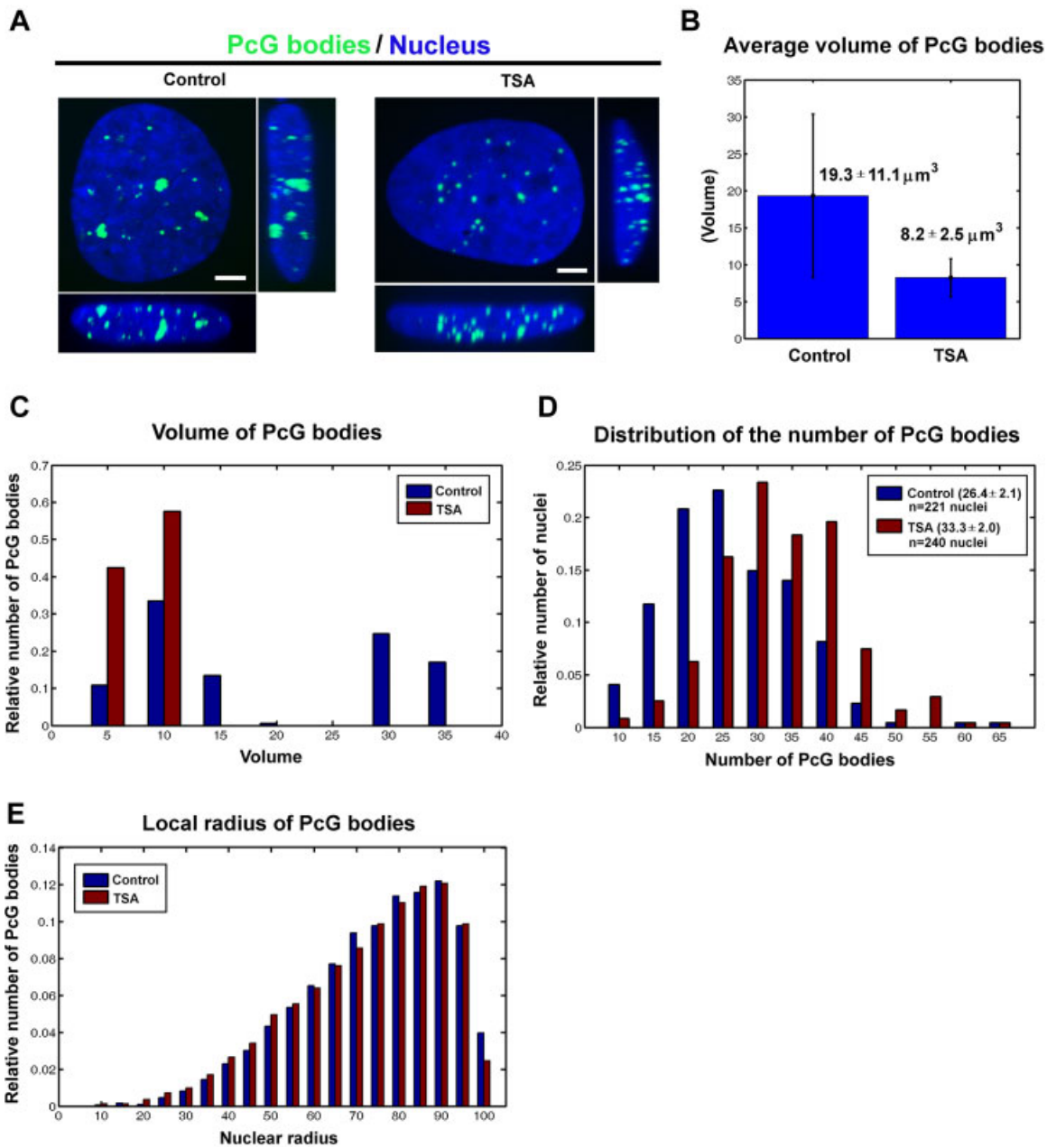

Fig. 7. Nuclear arrangement of PcG bodies. A: 3D-projections of PcG bodies in control and TSA-treated cells. Bar represents 2 μm. B: Average volume for PcG bodies calculated for >50 nuclei of control and TSA-treated U2OS cells. C: Relative number of PcG bodies ordered according to volume of PcG bodies in control and TSA-treated cells. D: Distribution of the number of PcG bodies in control and TSA-treated cells. TSA significantly increased the number of PcG bodies. E: Nuclear radial distribution of PcG bodies in control (blue bars) and TSA-treated (brown bars) cells.

Discussion

Here, we have shown that recruitment of BMI1 to UV-damaged chromatin took up to ~15 sec, which is more rapid than the recruitment of HP1β, which takes 100–800 sec (Ayoub et al., 2008; Luijsterburg et al., 2009; and Figs. 2A and 4A). Recruitment of HP1 to sites of damage was independent of the chromodomain (CD) of HP1, which suggests that this process is independent of the H3K9 trimethylation that is a binding partner for HP1 sub-types (Rice and Allis, 2001; Luijsterburg et al., 2009). Moreover, studies by Ayoub et al. (2008) show that phosphorylation of HP1β at Thr51 of its CD domain is important for mobilization and release from chromatin and for the recruitment of HP1β to sites of DNA damage. Interestingly, inhibition of casein kinase (CK2), an enzyme involved in DNA repair, suppresses Thr51 phosphorylation and HP1β mobilization (Ayoub et al., 2008). In addition, Baldeyron et al. (2011) showed that HP1α depletion leads to non-standard DNA repair and that HP1α recruitment to chromatin with DSBs requires the histone chaperone, p150CAF-1. These data imply that specific epigenetic events and biochemical modifications of chromatin-binding proteins, including HP1, are responsible for chromatin conformation and DNA repair, as well. Here, we show that increased accumulation of HP1β at UV-damaged chromatin occurs along with the pronounced recruitment of BMI protein. Moreover, this event is acetylation-dependent. Based on these results, BMI1 seems to be a potential binding partner for HP1β at UV-damaged chromatin, similar to what was observed in non-irradiated nuclei (Fig. 3). Just as HP1 proteins are recruited to UV-damaged chromatin irrespective of H3K9me3 (Luijsterburg et al., 2009), we have repeatedly observed that there is no pronounced accumulation of H3K27me3 at UV-damaged sites with markedly accumulated BMI1 (Fig. 2B). However, there was not an absence of H3K27me3; thus, it seems that the observed level of H3K27me3 could be sufficient for BMI1 binding at irradiated chromatin (Fig. 2B). Another important player for BMI1 recruitment to irradiated chromatin is poly-ADP-ribose polymerase (PARP; Chou et al., 2010) and accumulation of BMI1, together with RING2, to chromatin with DSBs contributes to the ubiquitylation of γH2AX (Ismail et al., 2010).

Here, we have also uncovered information about the dynamic properties of BMI1 in non-irradiated and irradiated cells. In UV-damaged chromatin, the recovery of BMI1 was quite fast (Fig. 5A). Especially, in non-irradiated cells, we confirmed the existence of two kinetically distinct pools of BMI1 of higher and lower dynamic activity. Similar phenomenon have been published by Hernández-Muñoz et al. (2005). We observed that the recovery time for BMI1 in PcG bodies of non-irradiated cells is slower compared to HP1 sub-types, in both euchromatin and heterochromatin domains (compare Figs. 4B with 5C or see Cheutin et al., 2003; Festenstein et al., 2003). For HP1, recovery time after photobleaching ($\tau 5_0$) is reached after several seconds, while for BMI1, it is close to 90–100 sec (Hernández-Muñoz et al., 2005; and Fig. 5C). Proper assembly of PcG bodies was found to be independent of DNA methyltransferase (DNMT)-associated histone deacetylase activity (Hernández-Muñoz et al., 2005). However, when we analyzed the kinetic properties for BMI1 after TSA treatment, we observed a longer recovery time required for BMI1 to diffuse into the bleached area (Fig. 5C). These experiments confirmed the existence of multiple dynamic fractions of BMI1 protein, the nuclear arrangement and function of which can be changed according to acetylation level.

Taken together, we showed that PcG-related BMI1 protein is recruited to UV-damaged chromatin immediately after micro-irradiation, which is followed by pronounced recruitment of GFP-HP1β. However, we are aware that the physiological significance of UV-micro irradiation may be limited, as is the biological significance of exogenous BMI1 expression. Nevertheless, in this experimental system, the recognition of UV-damaged chromatin by BMI1 was likely dependent on acetylation events, owing to the fact that histone hyperacetylation prevents increased accumulation of BMI1 and HP1β to irradiated chromatin (Figs. 2A and 4A). Conversely, it was shown that DNA repair is more efficient in hyperacetylated de-condensed nucleosomes (Ramanathan and Smerdon, 1986, 1989), but when BMI1 was recruited to UV-damaged region, we observed decreased global lysine acetylation (Fig. 2D). Using independent experimental approaches, our data have shown the importance of acetylation status for the DNA repair processes; thus, our results contribute to the knowledge of how the specific histone signature can influence DNA repair events.

Acknowledgments

This work was supported by the Ministry of Education Youth and Sports of the Czech Republic; the research projects LC535, LC06027, ME919, and by the Academy of Sciences of the Czech Republic; projects AVOZ50040702 and AVOZ50040507. Work was also supported by EU project COST TD09/05 and Marie Curie project PIRSES-GA-2010-269156-LCS. Some experiments were supported by the national COST-CZ project LD11020 and by Grant Agency of Czech Republic, project P302/10/1022. We are grateful to Dr. Paul Verbruggen (from Swammerdam Institute for Life Sciences University of Amsterdam, The Netherlands, in the group of Prof. Roel van Driel) who provided us with 3T3 cells stably expressing HP1β. We also thank to BioScience Writers Service (Houston, TX, USA) for linguistic revision of our manuscript.

Literature Cited

Ayoub N, Jeyasekharan AD, Bernal JA, Venkitaraman AR. 2008. HP1-beta mobilization promotes chromatin changes that initiate the DNA damage response. Nature 453:682–686.

Baldeyron C, Soria G, Roche D, Cook AJ, Almouzni G. 2011. HP1α recruitment to DNA damage by p150CAF-1 promotes homologous recombination repair. J Cell Biol 193:81–95.

Bantignies F, Grimaud C, Lavrov S, Gabut M, Cavalli G. 2003. Inheritance of Polycomb-dependent chromosomal interactions in Drosophila. Genes Dev 17:2406–2420.

Bártová E, Pacherník J, Harničarová A, Kovařík A, Kovaříková M, Hofmanová J, Skalníková M, Kozubek M, Kozubek S. 2005. Nuclear levels and patterns of histone H3 modification and HP1 proteins after inhibition of histone deacetylases. J Cell Sci 118:5035–5046.

Bártová E, Galiová G, Krejčí J, Harničarová A, Strašák L, Kozubek S. 2008. Epigenome and chromatin structure in human embryonic stem cells undergoing differentiation. Dev Dyn 237:3690–3702.

Buchenau P, Hodgson J, Strutt H, Arndt-Jovin DJ. 1998. The distribution of polycomb-group proteins during cell division and development in Drosophila embryos: Impact on models for silencing. J Cell Biol 141:469–481.

Cao R, Wang L, Wang H, Xia L, Erdjument-Bromage H, Tempst P, Jones RS, Zhang Y. 2002. Role of histone H3 lysine 27 methylation in Polycomb-group silencing. Science 298:1039–1043.

Cao R, Zhang Y. 2004. The functions of E(Z)/EZH2-mediated methylation of lysine 27 in histone H3. Curr Opin Genet Dev 14:155–164.

Cheutin T, McNairn AJ, Jenuwein T, Gilbert DM, Singh PB, Misteli T. 2003. Maintenance of stable heterochromatin domains by dynamic HP1 binding. Science 299:721–725.

Chou DM, Adamson B, Dephoure NE, Tan X, Nottke AC, Hurov KE, Gygi SP, Colaiácovo MP, Elledge SJ. 2010. A chromatin localization screen reveals poly (ADP ribose)-regulated recruitment of the repressive polycomb and NuRD complexes to sites of DNA damage. Proc Natl Acad Sci USA 107:18475–18480.

Czermin B, Melfi R, McCabe D, Seitz V, Imhof A, Pirrotta V. 2002. Drosophila enhancer of Zeste/ESC complexes have a histone H3 methyltransferase activity that marks chromosomal Polycomb sites. Cell 111:185–196.

Damelin M, Ooi SK, Bestor TH. 2006. Combing over heritable gene silencing. Nat Struct Mol Biol 13:100–101.

Dawson MA, Bannister AJ, Göttgens B, Foster SD, Bartke T, Green AR, Kouzarides T. 2009. JAK2 phosphorylates histone H3Y41 and excludes HP1alpha from chromatin. Nature 461:819–822.

Fernandez-Capetillo O, Lee A, Nussenzweig M, Nussenzweig A. 2004. H2AX: The histone guardian of the genome. DNA Repair (Amst) 3:959–967.

Festenstein R, Pagakis SN, Hiragami K, Lyon D, Verreaul A, Sekkali B, Kioussis D. 2003. Modulation of heterochromatin protein 1 dynamics in primary Mammalian cells. Science 299:719–721.

Fillingham J, Keogh MC, Krogan NJ. 2006. GammaH2AX and its role in DNA double-strand break repair. Biochem Cell Biol 84:568–577.

Harničarová A, Kozubek S, Pacherník J, Krejčí J, Bártová E. 2006. Distinct nuclear arrangement of active and inactive c-myc genes in control and differentiated colon carcinoma cells. Exp Cell Res 312:4019–4035.

Harničarová Horáková A, Bártová E, Galiová G, Uhlířová R, Matula P, Kozubek S. 2010. SUV39h-independent association of HP1beta with fibrillarin-positive nucleolar regions. Chromosoma 119:227–241.

Hernández-Muñoz I, Taghavi P, Kuijl C, Neefjes J, van Lohuizen M. 2005. Association of BMI1 with polycomb bodies is dynamic and requires PRC2/EZH2 and the maintenance DNA methyltransferase DNMT1. Mol Cell Biol 25:11047–11058.
Hong Z, Jiang J, Lan L, Nakajima S, Kanno S, Koseki H, Yasui A. 2008. A polycomb group protein, PHF1, is involved in the response to DNA double-strand breaks in human cell. Nucleic Acids Res 36:2939–2947.
Ismail IH, Andrin C, McDonald D, Hendzel MJ. 2010. BMI1-mediated histone ubiquitylation promotes DNA double-strand break repair. J Cell Biol 191:45–60.
Jacobs JJ, van Lohuizen M. 2002. Polycomb repression: From cellular memory to cellular proliferation and cancer. Biochim Biophys Acta 1602:151–161.
Kioussis D. 2005. Gene regulation: Kissing chromosomes. Nature 435:579–580.
Kozubek M, Kozubek S, Lukášová E, Marečková A, Bártová E, Skalníková M, Jergová A. 1999. High-resolution cytometry of FISH dots in interphase cell nuclei. Cytometry 36: 279–293.
Kruhlak MJ, Celeste A, Dellaire G, Fernandez-Capetillo O, Müller WG, McNally JG, Bazett-Jones DP, Nussenzweig A. 2006. Changes in chromatin structure and mobility in living cells at sites of DNA double-strand breaks. J Cell Biol 172:823–834.
Kuzmichev A, Nishioka K, Erdjument-Bromage H, Tempst P, Reinberg D. 2002. Histone methyltransferase activity associated with a human multiprotein complex containing the Enhancer of Zeste protein. Genes Dev 16:2893–2905.
Kuzmichev A, Jenuwein T, Tempst P, Reinberg D. 2004. Different EZH2-containing complexes target methylation of histone H1 or nucleosomal histone H3. Mol Cell 14: 183–193.
Laible G, Wolf A, Dorn R, Reuter G, Nislow C, Lebersorger A, Popkin D, Pillus L, Jenuwein T. 1997. Mammalian homologues of the Polycomb-group gene Enhancer of zeste mediate gene silencing in Drosophila heterochromatin and at *S. cerevisiae* telomeres. EMBO J 16:3219–3232.
Lanctôt C, Cheutin T, Cremer M, Cavalli G, Cremer T. 2007. Dynamic genome architecture in the nuclear space: Regulation of gene expression in three dimensions. Nat Rev Genet 8:104–115.
Luijsterburg MS, Dinant C, Lans H, Stap J, Wiernasz E, Lagerwerf S, Warmerdam DO, Lindh M, Brink MC, Dobrucki JW, Aten JA, Fousteri MI, Jansen G, Dantuma NP, Vermeulen W, Mullenders LH, Houtsmuller AB, Verschure PJ, van Driel R. 2009. Heterochromatin protein 1 is recruited to various types of DNA damage. J Cell Biol 185:577–586.
Lund AH, van Lohuizen M. 2004. Polycomb complexes and silencing mechanisms. Curr Opin Cell Biol 16:239–246.
Minc E, Allory Y, Worman HJ, Courvalin JC, Buendia B. 1999. Localization and phosphorylation of HP1 proteins during the cell cycle in mammalian cells. Chromosoma 108:220–234.
Minc E, Allory Y, Courvalin JC, Buendia B. 2001. Immunolocalization of HP1 proteins in metaphasic mammalian chromosomes. Methods Cell Sci 23:171–174.
Müller J, Hart CM, Francis NJ, Vargas ML, Sengupta A, Wild B, Miller EL, O'Connor MB, Kingston RE, Simon JA. 2002. Histone methyltransferase activity of a Drosophila Polycomb group repressor complex. Cell 111:197–208.
Muratani M, Gerlich D, Janicki SM, Gebhard M, Eils R, Spector DL. 2002. Metabolic-energy-dependent movement of PML bodies within the mammalian cell nucleus. Nat Cell Biol 4:106–110.
Plath K, Fang J, Mlynarczyk-Evans SK, Cao R, Worringer KA, Wang H, de la Cruz CC, Otte AP, Panning B, Zhang Y. 2003. Role of histone H3 lysine 27 methylation in X inactivation. Science 300:131–135.
Ramanathan B, Smerdon MJ. 1986. Changes in nuclear protein acetylation in UV-damaged human cells. Carcinogenesis 7:1087–1094.
Ramanathan B, Smerdon MJ. 1989. Enhanced DNA repair synthesis in hyperacetylated nucleosomes. J Biol Chem 264:11026–11034.
Rice JC, Allis CD. 2001. Histone methylation versus histone acetylation: New insights into epigenetic regulation. Curr Opin Cell Biol 13:263–273.
Ringrose L, Paro R. 2004. Epigenetic regulation of cellular memory by the Polycomb and Trithorax group proteins. Annu Rev Genet 38:413–443.
Saurin AJ, Shiels C, Williamson J, Satijn DP, Otte AP, Sheer D, Freemont PS. 1998. The human polycomb group complex associates with pericentromeric heterochromatin to form a novel nuclear domain. J Cell Biol 142:887–898.
Sauvageau M, Sauvageau G. 2008. Polycomb group genes: Keeping stem cell activity in balance. PLoS Biol 6:e113.
Sewalt RG, Lachner M, Vargas M, Hamer KM, den Blaauwen JL, Hendrix T, Melcher M, Schweizer D, Jenuwein T, Otte AP. 2002. Selective interactions between vertebrate polycomb homologs and the SUV39H1 histone lysine methyltransferase suggest that histone H3-K9 methylation contributes to chromosomal targeting of Polycomb group proteins. Mol Cell Biol 22:5539–5553.
Silva J, Mak W, Zvetkova I, Appanah R, Nesterova TB, Webster Z, Peters AH, Jenuwein T, Otte AP, Brockdorff N. 2003. Establishment of histone H3 methylation on the inactive X chromosome requires transient recruitment of Eed-Enx1 polycomb group complexes. Dev Cell 4:481–495.
Tóth KF, Knoch TA, Wachsmuth M, Frank-Stöhr M, Stöhr M, Bacher CP, Müller G, Rippe K. 2004. Trichostatin A-induced histone acetylation causes decondensation of interphase chromatin. J Cell Sci 117:4277–4287.
Uhlířová R, Harničarová Horáková A, Galiová G, Legartová S, Matula P, Fojtová M, Vařecha M, Amrichová J, Vondráček J, Kozubek S, Bártová E. 2010. SUV39h- and A-type Lamin-dependent telomere nuclear rearrangement. J Cell Biochem 109:915–926.